

# Comparing Stochastic Point-Source and Finite-Source Ground-Motion Simulations: SMSIM and EXSIM

by David M. Boore

**Abstract** Comparisons of ground motions from two widely used point-source and finite-source ground-motion simulation programs (SMSIM and EXSIM) show that the following simple modifications in EXSIM will produce agreement in the motions from a small earthquake at a large distance for the two programs: (1) base the scaling of high frequencies on the integral of the squared Fourier acceleration spectrum; (2) do not truncate the time series from each subfault; (3) use the inverse of the subfault corner frequency for the duration of motions from each subfault; and (4) use a filter function to boost spectral amplitudes at frequencies near and less than the subfault corner frequencies. In addition, for SMSIM an effective distance is defined that accounts for geometrical spreading and anelastic attenuation from various parts of a finite fault. With these modifications, the Fourier and response spectra from SMSIM and EXSIM are similar to one another, even close to a large earthquake ( $M$  7), when the motions are averaged over a random distribution of hypocenters. The modifications to EXSIM remove most of the differences in the Fourier spectra from simulations using pulsing and static subfaults; they also essentially eliminate any dependence of the EXSIM simulations on the number of subfaults. Simulations with the revised programs suggest that the results of [Atkinson and Boore \(2006\)](#), computed using an average stress parameter of 140 bars and the original version of EXSIM, are consistent with the revised EXSIM with a stress parameter near 250 bars.

## Introduction

Stochastic models of the seismic source and wave propagation have been used to simulate ground motions for many years (e.g., [Boore, 1983, 2003](#)). One widely used simulation program is SMSIM ([Boore, 2005a](#)). This is a point-source simulation program in that no information about the fault geometry is used in the calculations. As such, it is not obvious that the program is useful for simulations close to large earthquakes (although using the closest distance to the rupture surface rather than the hypocentral distance helps offset the point-source limitation). To overcome the limitation of the point-source model, several models have been published that sum the motions from subfaults distributed over a fault surface, where the motions from each subfault are often given by the point-source stochastic method simulation. Formally, stochastic finite-source models should be primarily used at frequencies above those for which deterministic simulations are valid (usually about 0.5 to 1.0 Hz). In spite of this apparent limitation, however, the stochastic method can provide simulations that are in good agreement with observations over much of the frequency range of engineering interest (e.g., [Hartzell \*et al.\*, 1999](#); [Motazedian and Atkinson, 2005a](#)). Two readily available stochastic finite-fault simulation programs are FINSIM ([Beresnev and Atkinson, 1998](#))

and EXSIM ([Motazedian and Atkinson, 2005a](#)), the latter being an updated version of the former. The time series from each subfault in these programs is based on the methods in SMSIM. Although the three programs have been used in many applications, a careful comparison of the SMSIM and EXSIM/FINSIM simulations has not been published (from now on I will refer only to EXSIM). Such a comparison was the initial motivation for the research described in this article. As the research progressed, however, a number of revisions to EXSIM were suggested, some minor and some not so minor; in addition, an important modification was made to SMSIM. Thus, this article is focused more on revisions to the EXSIM and SMSIM programs than on a comparison of the SMSIM and EXSIM simulations, although a number of such comparisons are in the article and were of essential importance in revealing the need for the revisions to EXSIM and SMSIM discussed here. An important revision to SMSIM is to use an effective distance that is easily computed, given the fault size and orientation, the location of the site with respect to the fault, and the geometrical spreading and anelastic attenuation of the waves. For EXSIM there are two main modifications, one influencing high-frequency motions and one impacting low- to intermediate-frequency motions.

The two modifications were controlled by the requirement that motions from EXSIM be in close agreement with those from SMSIM far from small earthquakes. The modifications to EXSIM and to SMSIM also result in ground motions that are in reasonably close agreement with one another near large earthquakes, at least for an average of the motions from a random distribution of hypocenters over the fault surface. The need for the EXSIM correction at low and intermediate frequencies probably exists for any finite-fault model in which random motions from subfaults are added with appropriate delays and amplitude scaling to simulate the motions from an extended rupture; thus, the suggested modification may have application to more than just EXSIM.

The version of EXSIM used in the comparison is a revision of the publically available release version 1.0, 10 October 2005. I needed to make several important revisions to this program to allow comparisons with the SMSIM results that were not marred by differences due to easily corrected limitations or assumptions in the distributed version of EXSIM; these initial revisions to EXSIM are described in the [Appendix](#). The two main revisions discussed in the [Appendix](#) are (1) base the scaling of high-frequency motions on the integral of the squared acceleration spectrum rather than the integral of the squared velocity spectrum, and (2) remove the truncation of the subfault time series (which can result in long-period errors). All simulations are for the

eastern North America hard-rock model of [Atkinson and Boore \(2006\)](#), although the essential findings hold for other models, including those for western North America on soft-rock sites. Thus, none of the results in this article are dependent on the specific model used in the simulations. [Tables 1 and 2](#) give the essential input parameters for the simulations. Plots of response spectra are generally in terms of pseudo-velocity response spectra (PSV) because a smaller range of the ordinate axis is needed than for pseudoacceleration or displacement response spectra, thus allowing more resolution in comparisons of response spectra computed using different programs or different input assumptions.

I recognize that there is a growing trend toward using broadband simulations, in which deterministic simulations at low frequencies are combined with stochastic simulations at high frequencies (e.g., [Graves and Pitarka, 2004](#); [Frankel, 2009](#); [Ameri et al., 2009](#)). Such methods have the potential of more accurately simulating directivity effects at low frequencies than the stochastic finite-fault methods. Purely stochastic simulations still have important uses, however. For example, they can be used for generic or region specific rather than path specific applications, for which the average motions from a suite of earthquakes rather than a scenario earthquake are desired. One application for such simulations is to generate synthetic data sets from which ground-motion prediction equations can be produced at

Table 1  
Parameters Used in Simulations

Parameter	Value
Shear-wave velocity ( $V_S$ )	3.7 km/sec
Density ( $\rho$ )	2.8 gm/cm <sup>3</sup>
Geometric spreading $R^b$ : $b =$	-1.3 (0–70 km) +0.2 (70–140 km) -0.5 (> 140 km)
Distance dependence of duration, $dR$ , $d =$	(0–10 km) +0.16 (10–70 km) -0.03 (70–130 km) +0.04 (> 130 km)
Quality factor	$Q = \max[1000, 893f^{0.32}]$
$\kappa_0$	0.005 sec
Fault plane orientation	Vertical, intersecting the Earth's surface, except as noted in <a href="#">Figure 11</a>
Fault length and width	<b>M 5</b> : 3.6 km $\times$ 1.2 km <b>M 7</b> : 29.4 km $\times$ 9 km
Stress parameter	140 bars
Rupture propagation speed	$0.8V_S$
Type of subfault	Static (constant corner frequency for all subfaults), unless otherwise noted
Subfault source duration (also known as rise time)	$1/f_{0sf}$ , unless otherwise noted, where $f_{0sf}$ is the subfault corner frequency; this changes from subfault-to-subfault for a pulsing source.
Slip distribution	Uniform
Type of window	Tapered box, unless otherwise noted
EXSIM simulations: Original EXSIM taper function was applied for frequencies less than $f_{0sf}/15$	
EXSIM simulations: 100 random hypocenters, with 10 simulations per hypocenter. FAS and response spectra are rms average and geometrical mean of the 1000 realizations, respectively	

Table 2  
Crustal plus Site Amplifications (Linear Interpolation  
between Tabulated Values)

Frequency (Hz)	Amplification
0.5	1
1	1.13
2	1.22
5	1.36
10	1.41

frequencies of engineering interest, as in [Atkinson and Boore \(2006\)](#).

### Low Motions from EXSIM Simulations Compared with Those from SMSIM

Comparisons of Fourier acceleration spectra (FAS) from EXSIM and SMSIM simulations for small and large earthquakes at close and far distances reveal that the FAS from EXSIM are substantially below the FAS from SMSIM (this after correcting for differences at high frequencies as discussed in the [Appendix](#)). This is shown in [Figure 1](#) for a small magnitude ( $M$  5) at a substantial distance (160 km). The corner frequency  $f_0$  for each subfault was chosen to be constant in the EXSIM simulations. The assumption of a constant corner frequency for all subfaults is referred to in EXSIM as the static subfault assumption. The static source is equivalent to the simulation method used in FINSIM (D. Motazedian, written communication, 2009), and results in a strong dependence of the motions on the number of subfaults, as shown in [Figure 1](#). One of the major improvements of EXSIM over FINSIM was the introduction of the pulsing source, in which the corner frequency of each subfault is proportional to the number of subfaults active at a given time. The pulsing source substantially reduces the dependence of the motions on the number of subfaults, as shown by the dashed lines in [Figure 1](#). The point I want to emphasize in [Figure 1](#) is the discrepancy between the motions from EXSIM and from SMSIM, not the dependence of the EXSIM motions on subfault size. I used a static source in this and the next few figures to simplify some of the analysis to follow. The vertical gray lines in [Figure 1](#) show the corner frequencies of the simulated event and the subfaults used in the two approximations of the finite source (not shown are EXSIM results for no subdivision of the fault; the EXSIM results in that case are the same as those from SMSIM). The results are root mean square (rms) means of 10 simulations for each of 100 randomly located hypocenters.

It is clear from [Figure 1](#) that there is a substantial and consistent underestimation of the FAS from the EXSIM simulations. This underestimation is likely a result of incoherent summation of the subfault time series. At low frequencies coherent summation will give a FAS equal to  $N$  times the FAS of the subfaults (by assuming static subfaults, I guarantee that the subfault Fourier amplitude spectra are essentially identical to one another, although that will not be true of the phase spectra), whereas incoherent summation will give a

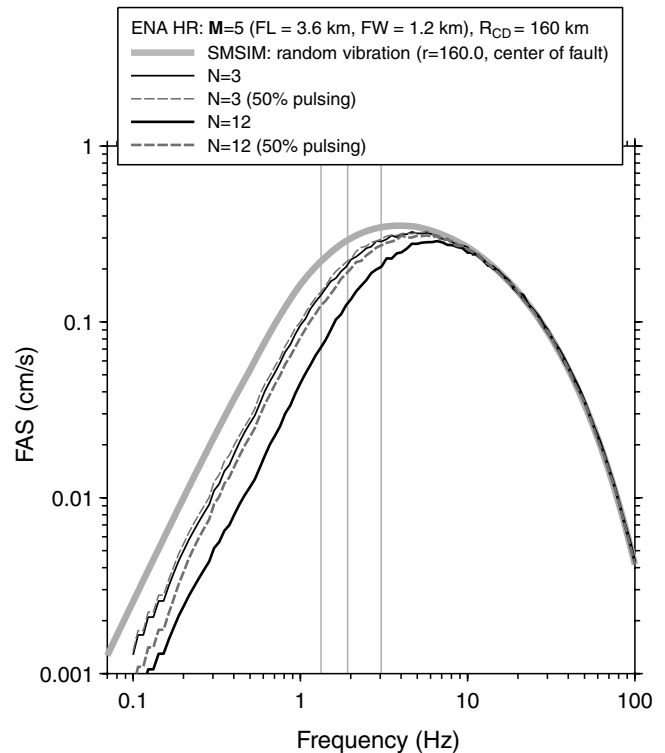


**Figure 1.** Fourier acceleration spectra (FAS) from SMSIM and EXSIM simulations, using the revised EXSIM program described in the [Appendix](#), in addition to using the inverse of the subfault corner frequency as the subfault source duration. A static source was used for EXSIM, in which the corner frequency for each subfault is the same, given by the standard relation between corner frequency, seismic moment, and stress parameter (e.g., equation 4 in [Boore, 2003](#)). EXSIM simulations are shown for subdivisions of the rupture surface into 3 and 12 subfaults. The vertical gray lines are the corner frequencies of the target event and the subfaults corresponding to 3 and 12 subdivisions of the main fault, respectively. The dashed gray lines show the results for a 50% pulsing fault.

FAS equal to  $\sqrt{N}$ . Thus, one way of testing whether the underestimation is due to incoherent summation is to multiply the EXSIM FAS by  $\sqrt{N}$ . The results of doing so are shown in [Figure 2](#), where it is clear that the underestimation of the FAS by EXSIM is equal to  $1/\sqrt{N}$ , thus strongly suggesting that the underestimation is due to incoherent summation.

Before discussing a procedure for correcting the underestimation, I show an interesting result from [Joyner and Boore \(1986\)](#). In that article an equation was derived for the FAS resulting from adding  $N$  identical complex Fourier acceleration spectra scaled by a factor  $H$  when the time series corresponding to the individual subfaults are distributed randomly over a duration  $T$  (note that [Joyner and Boore, 1986](#) use  $\eta$  and  $\kappa$  rather than  $N$  and  $H$ ; I am using the latter notation to avoid confusion with the diminution parameter  $\kappa$  and to be consistent with the notation for the high-frequency scaling factor used in [Motazedian and Atkinson, 2005a](#)). The assumptions leading to [Joyner and Boore's](#) equation (1) are similar to the EXSIM simulation method using a static source, except that in EXSIM the complex Fourier acceleration

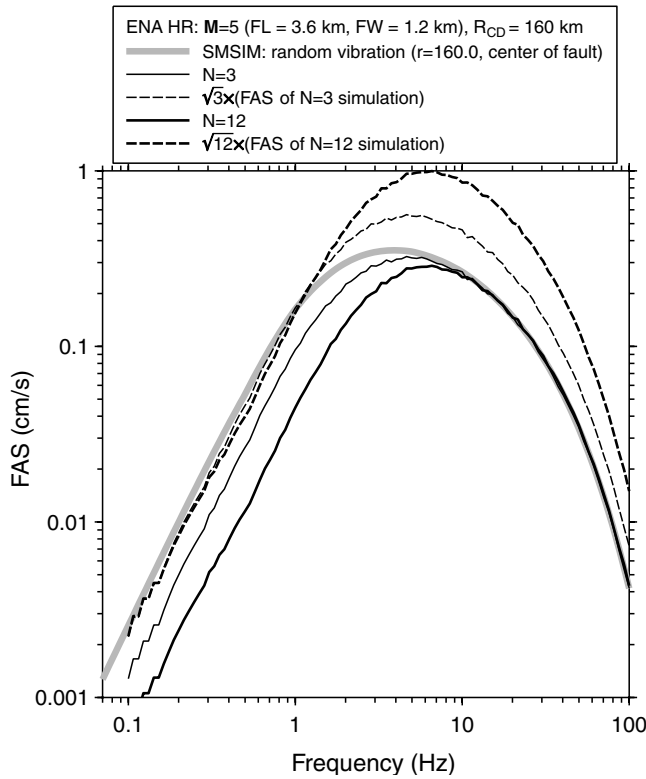


**Figure 2.** Fourier acceleration spectra (FAS) from SMSIM and EXSIM simulations, as in Figure 1, but the FAS from EXSIM have been multiplied by  $\sqrt{N}$ .

spectra of the subfaults are not identical (and thus add incoherently at all frequencies, as just shown). Figure 3 shows the result of multiplying the subfault FAS by the factor given in equation 1 of Joyner and Boore (1986), where the product has been scaled to match the SMSIM FAS at 10 Hz. The values used for  $N$  and  $H$  are those from EXSIM, not those from Joyner and Boore (1986). As a result, there is an underestimation of the low-frequency FAS obtained using Joyner and Boore's equation, compared with the FAS given by SMSIM (which has the correct low-frequency level, as determined by the seismic moment corresponding to  $M$  5). This underestimation was recognized by Motazedian and Atkinson (2005a) on the basis of the theory underlying EXSIM; they used an *ad hoc* taper function in an attempt to correct for the underestimation (note that this *ad hoc* correction is for a factor in addition to the effect of incoherent summation; it does not correct for the incoherent summation, which is the dominant effect at frequencies less than about 0.8 Hz in Figure 3). In practice their correction has little effect, as it only starts for frequencies less than  $1/15$  the corner frequencies of the subfaults. The dashed lines in Figure 3 would have had low-frequency asymptotes that are the same as the target FAS if  $N$  and  $H$  had been computed from the equations in Joyner and Boore (1986) (this is not shown for clarity of presentation). Figure 3 shows that an underestimation of the target FAS is expected for a range of frequencies even if identical complex spectra are summed.

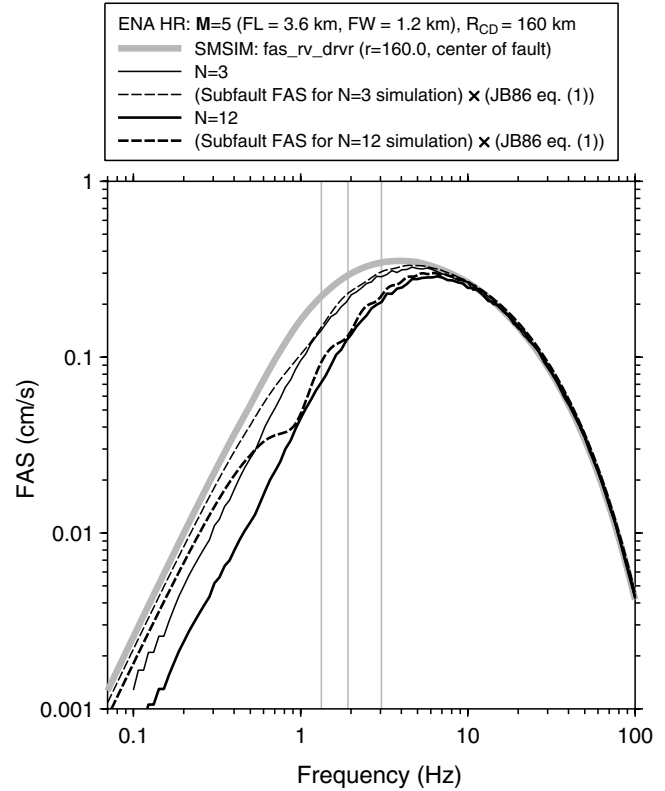


**Figure 3.** Fourier acceleration spectra (FAS) from SMSIM and EXSIM simulations, as in Figure 1, but with the EXSIM FAS for each subfault multiplied by the factor given in equation (1) of Joyner and Boore (1986) (using  $N$  and  $H$  from EXSIM) and normalized to the SMSIM value at 10 Hz.

If the view is taken that the EXSIM results should be the same as the SMSIM point-source results for a small earthquake at a substantial distance (this is the key assumption in what follows), then two modifications are needed to EXSIM: (1) correct for the underestimation at intermediate frequencies, resulting from the summation-effect predicted by Joyner and Boore's equation (1); (2) correct for the underestimation at low frequencies resulting from incoherent summation. Frankel (1995) recognized that summing subfault motions would lead to underestimation of the target FAS for frequencies less than the subfault corner frequency (see his figure 2), and he used a filter to flatten out the subfault FAS at frequencies between the target and the subfault corner frequencies. Frankel's filter is given by the ratio of the simple source spectra for the main (target) event divided by that for the subfault. (Hisada, 2008, also recognized the problem but he overcame the incoherent summation by requiring the phase of the spectra to approach a constant value of 0.0 at low frequency; others, such as Irikura and Kamae, 1994, have used the ratio of the transforms of box functions for the filter). I used a modification of Frankel's filter given by

$$S(f) = C \frac{1 + (f/f_{0sf})^2}{1 + (f/f_{0eff})^2}, \quad (1)$$

where

$$C = \frac{\sqrt{N}}{H}, \quad (2)$$

and

$$f_{\text{0eff}} = f_{\text{0sf}} \frac{1}{\sqrt{C}}. \quad (3)$$

$H$  is the high-frequency scaling factor discussed in the Appendix and  $N$  is the number of subfaults. In equations (1), (2), and (3),  $H$  and  $f_{\text{0sf}}$ , and thus  $C$ ,  $f_{\text{0eff}}$ , and  $S$ , will generally be different for each subfault  $i, j$ ; the subfault subscripts have been omitted for clarity.

Frankel's filter corresponds to equation (1), but with the corner frequency  $f_{\text{0main}}$  of the main (target) event used in the denominator. I had to use  $f_{\text{0eff}}$  rather than  $f_{\text{0main}}$  in equation (1) in order to satisfy these two constraints:

$$S(f) \rightarrow 1 \quad (4)$$

at high frequency, and

$$S(f) \rightarrow \sqrt{N}/H \quad (5)$$

at low frequencies (the inverse of the high-frequency scaling factor  $H$  is needed for the moment of the simulated event to be equal to the specified moment; this is the theoretical correction recognized by Motazedian and Atkinson, 2005a); in practice,  $S > 1$  at low frequencies. I revised EXSIM to include the filter function  $S(f)$ . The FAS and PSV from the original and revised EXSIM are compared with those from

SMSIM in Figure 4 for  $M$  5 at 160 km. Now the EXSIM and SMSIM simulations are in close agreement with one another, and the dependence of the EXSIM results on the number of subfaults has been removed. Clearly, the revision to EXSIM accomplishes my goals: the low-frequency intercept is now correct, the underestimation due to incoherent summation no longer exists, and the EXSIM FAS agrees with that for SMSIM for a small earthquake at a large distance.

#### Modification to SMSIM: $R_{\text{EFF}}$

The comparisons in the previous section were for a small magnitude at a large distance, where it is reasonable to expect that the point-source simulations of EXSIM should be close to those of the finite-source EXSIM simulations. This agreement should not necessarily be expected, however, close to a large earthquake. One of the most important differences between the point and the extended source simulations is that the motions from the extended source are arriving from parts of the fault at a range of distances from the site. It is possible, however, to modify the single distance used in the point-source simulation to capture the effect of the range of distances. The idea is straightforward and has been used by previous authors (e.g., Singh *et al.*, 1989; Cocco and Boatwright, 1993; Ohno *et al.*, 1993; Andrews, 2001). The simplest modification assumes random hypocenter locations on an extended fault (this is a reasonable assumption for applications in which mean motions are desired, as in developing the ground-motion prediction equations of Atkinson and Boore, 2006; the assumption could be modified to account for the nonuniform distribution of hypocenters found in studies such as Mai *et al.*, 2005, but neither EXSIM or SMSIM have incorporated nonuniform distributions of

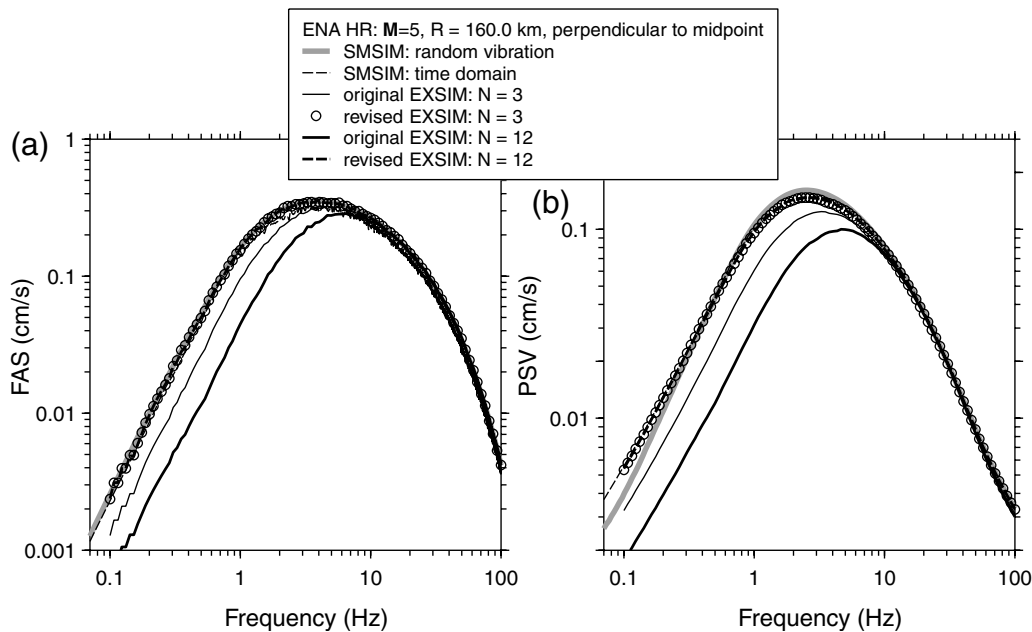


**Figure 4.** (a) FAS and (b) PSV for  $M$  5 at 160 km from SMSIM and the original and revised versions of EXSIM. Results are shown both for time-domain and random-vibration SMSIM calculations, to demonstrate that there is little difference in the results.

hypocenter locations as of this date). Then assuming that the contributions from the subfaults add incoherently, the following equation can be used to obtain an effective distance to be used in the place of the closest distance to the fault in the SMSIM calculations:

$$G(R_{\text{EFF}}) \exp(-\pi f_Q R_{\text{EFF}} / Q(f_Q) V_S) = \left[ \frac{1}{N} \sum_{i=1}^N \{G(R_i) \exp(-\pi f_Q R_i / Q(f_Q) V_S)\}^2 \right]^{1/2}, \quad (6)$$

where  $G(R)$  is the geometrical spreading function used in the SMSIM calculations. In equation (6),  $R_i$  is the distance from the site to the  $i$ th subfault, and  $R_{\text{EFF}}$  is the effective distance obtained by solving the equation (the right side is calculated and then  $R_{\text{EFF}}$  is found iteratively such that the left side of the equation equals the right side of the equation). In the anelastic attenuation function parameterized by  $Q(f)$ ,  $V_S$  is the shear-wave velocity and  $f_Q$  is a reference frequency. In the application used to illustrate this article, the geometrical spreading was that used by Atkinson and Boore (2006), based on Atkinson (2004). This geometrical spreading increases between 70 and 140 km, as shown in Figure 5. This increase will lead to difficulty in finding  $R_{\text{EFF}}$  if  $Q$  is not considered, because for a range of  $G(R)$  there will be three values of  $R$  corresponding to a single value of  $G$ . Introducing the anelastic attenuation and choosing  $f_Q$  high enough will remove the multivalued nature of the decay function, as shown in Figure 5. In this article I use  $f_Q = 10$  Hz; the results are not sensitive to the choice of  $f_Q$ .

The ratio of the effective distance  $R_{\text{EFF}}$  to the closest distance  $R_{\text{CD}}$  is shown in Figure 6 for vertical faults with

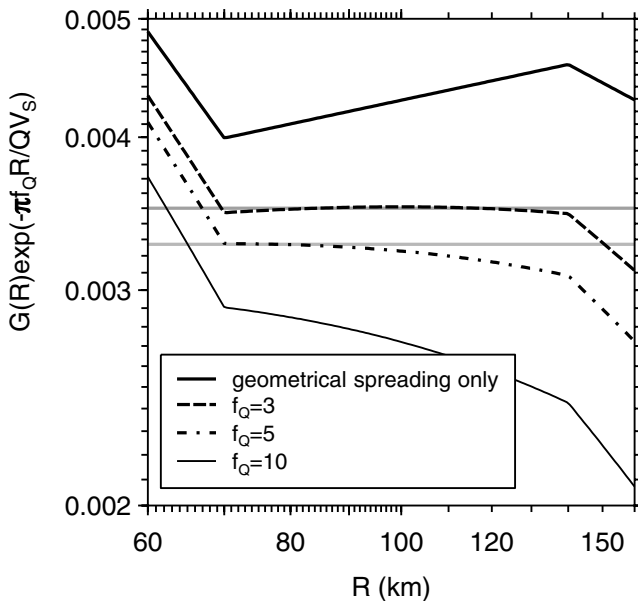


**Figure 5.** The distance decay from geometrical spreading alone and geometrical spreading and anelastic attenuation for frequencies of 3, 5, and 10 Hz, for the distance region around which the geometrical spreading alone increases with distance.

magnitudes of 5 and 7. The two graphs are for sites in directions perpendicular to the midpoint of the surface intersection of the fault and along the fault strike. Using  $R_{\text{EFF}}$  rather than  $R_{\text{CD}}$  in SMSIM results in a major improvement in the comparison of the point-source and extended source simulations, as shown in Figure 7 for a site close to an **M** 7 fault. In that figure the FAS are very similar for the EXSIM and SMSIM simulations, even close to a large earthquake, while there are some differences in the PSV. These differences in PSV increase with frequency, where the difference is a factor of 1.3 at 10 Hz. The durations used for the time-series simulations can differ between the two types of simulations, resulting in different PSVs even if the FASs are similar. This is discussed in more detail in the next section.

Using  $R_{\text{EFF}}$  rather than  $R_{\text{CD}}$  is clearly an important modification in applications of the SMSIM point-source simulations. The difference between using the closest distance or the effective distance is almost a factor of 7 close to the **M** 7 earthquake in the along-strike direction; this is much larger than the difference between the EXSIM motions and those from SMSIM when  $R_{\text{EFF}}$  is used in the simulations. It is interesting to note that Scherbaum *et al.* (2006) found that point-source stochastic simulations gave a better fit to motions from empirical ground-motion prediction equations if hypocentral distance rather than closest distance was used in the point-source simulations. This is probably an expression of what I find here.

#### Calculation of Subfault Corner Frequency and Duration in EXSIM

The distributed version of EXSIM uses the stochastic method as implemented in SMSIM to generate the time series for each subfault, except for one thing: the source portion of the duration of the subfault time series (referred to in EXSIM as rise time) is given by

$$\sqrt{\frac{dl \times dw}{\pi}} / v_{\text{rup}}, \quad (7)$$

where  $dl$  and  $dw$  are the subfault length and width and  $v_{\text{rup}}$  is the rupture velocity. SMSIM sets the source duration to

$$1/f_{\text{osf}}, \quad (8)$$

where  $f_{\text{osf}}$  is the subfault corner frequency, which is a function of the seismic moment and the stress parameter. These two durations are not necessarily the same, and as a result the various ground-motion intensity parameters can differ for two ground motions with the same Fourier acceleration spectra, depending on which definition is used for the subfault source duration. The total duration of the ground motion is made up of a source and a path effect, with the latter generally increasing with distance. For this reason, the sensitivity of ground-motion intensity parameters to the source duration is greatest at close distances. Examples of the

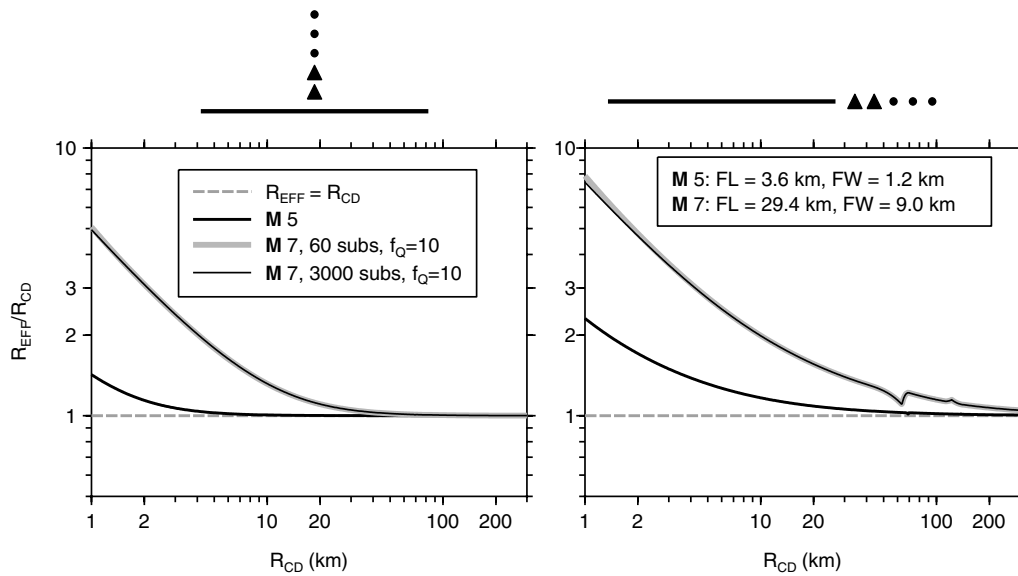


**Figure 6.** Ratio of effective distance to closest distance for **M 5** and **7** for sites along lines (a) perpendicular and (b) parallel to a vertical fault. The bumps in the **M 7** curves in (b) are related to the changes in slope of the geometrical spreading factor at 70 and 140 km: for  $R_{CD}$  near 70 and 140 km some subfaults may be at distances greater than or less than the hinge distances in the geometrical spreading factor, and the combination of the geometrical spreading and attenuation functions for the set of subfaults results in the bumps in the curve when  $R_{EFF}$  is computed from equation (6). The relative geometry of the fault and the sites is shown by the sketch at the top of each graph.

dependence of the PSV on the duration definition are shown in Figure 8. In this figure both a static and a pulsing source are used, where the static source (as used in EXSIM) has the same corner frequency for each subfault, whereas the pulsing subfaults have corner frequencies that are inversely propor-

tional to the number of subfaults pulsing at the same time (see [Motazedian and Atkinson, 2005a](#), for an explanation). The corner frequencies for the pulsing sources are lower than those for static subfaults, often by a significant amount.

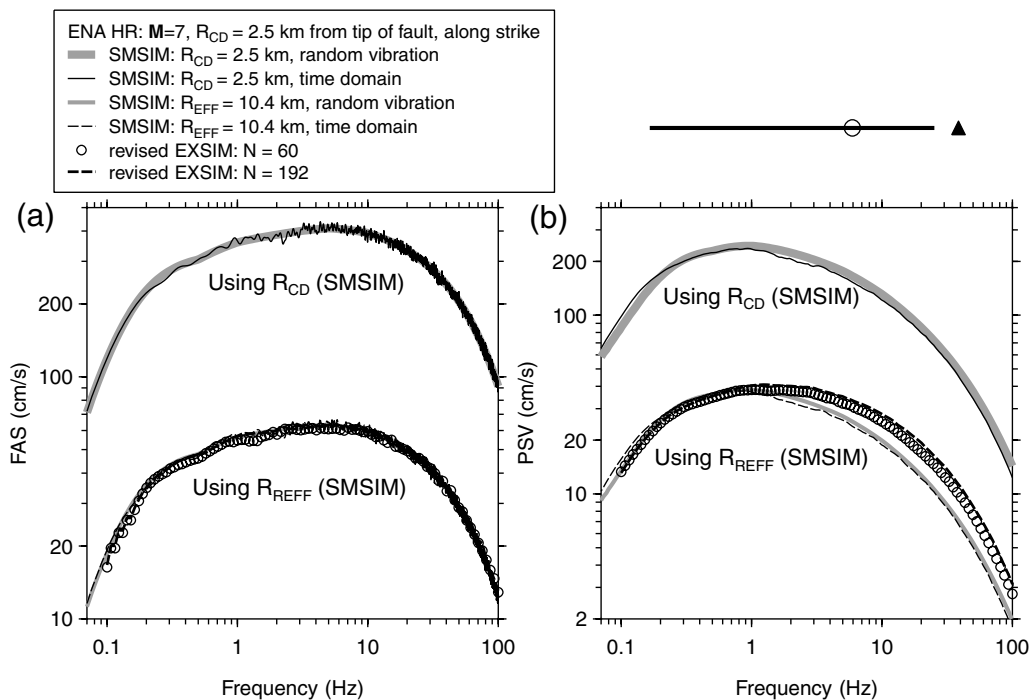


**Figure 7.** (a) FAS and (b) PSV for **M 7** at  $R_{CD} = 2.5$  km from the tip of a vertical fault in the along-strike direction. The EXSIM simulations used the revised program with the fault subdivided into 60 and 192 subfaults. The SMSIM simulations are shown for random vibration and for time-domain calculations, using both  $R_{CD}$  and  $R_{EFF}$ . The relative geometry of the fault and the site is shown by the sketch at the top of the right-hand graph; the open circle is a source at the distance  $R_{EFF}$ .

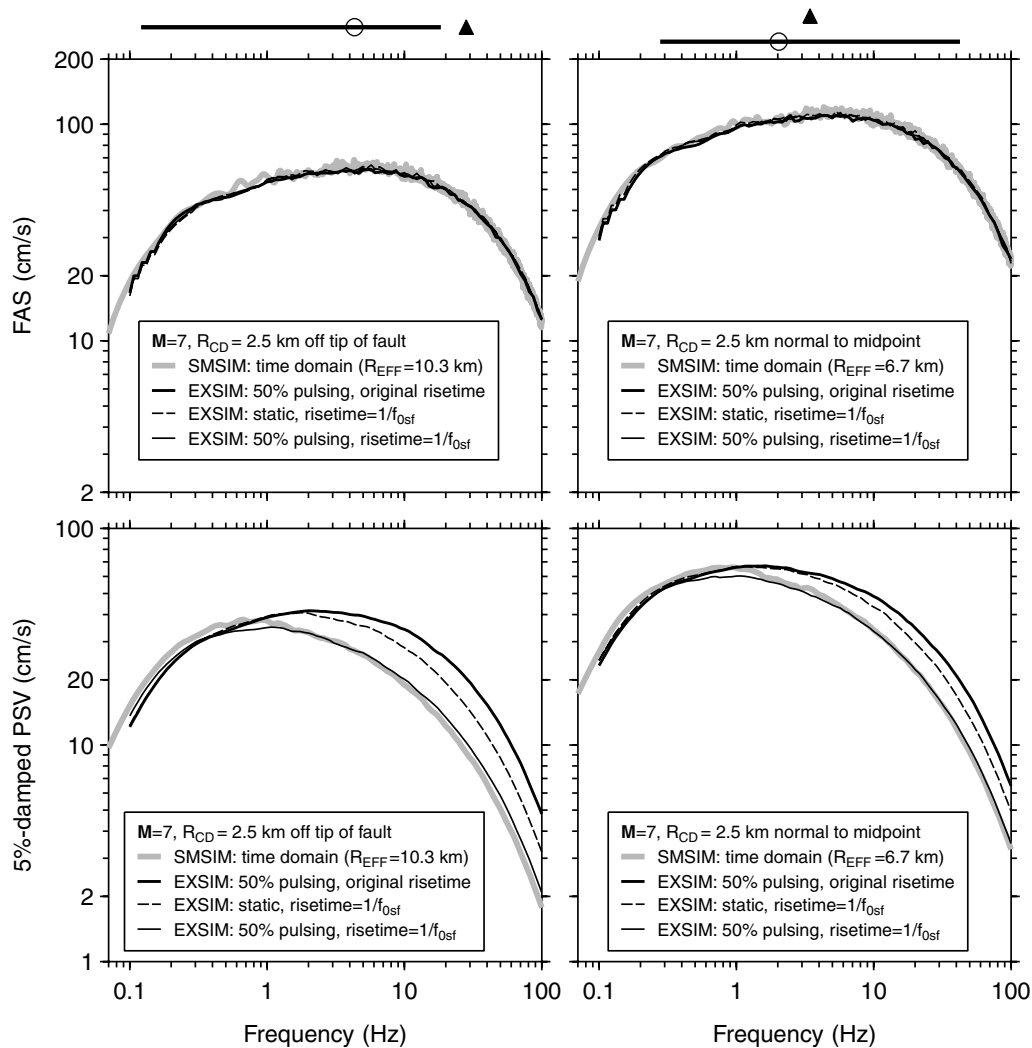


**Figure 8.** Fourier spectra (top row) and pseudovelocity response spectra (bottom row) for sites 2.5 from the tip of the fault (left column) and from the midpoint of the surface projection of the fault (right column), showing the effect of different choices for the subfault corner frequency and rise time. The relative geometries of the fault and the site are shown by the sketches at the top of the figure; the open circle is a source at the distance  $R_{\text{EFF}}$ . An exponential window was used for both the EXSIM and SMSIM calculations, with parameters  $\varepsilon = 0.2$ ,  $\eta = 0.05$ , and  $f_{T_{\text{gm}}} = 2.0$  (see Boore, 2003, for the meaning of these parameters).

The effect of the subfault duration, corner frequency assumption on simulated acceleration time series is illustrated in Figure 9. The distance to the fault is short enough that the path component of duration is minimal. To aid in assessing the durations, the normalized cumulative integral of the squared acceleration time series are also included in the figure, along with the 75% to 5% bounds used in the measure of duration proposed by Ou and Herrmann (1990). Although the time series shown in that figure are for only the first of the 100 randomly located hypocenters used to generate the spectra shown in Figure 8, the differences in average response spectra are consistent with the relative durations of the motions in Figure 9. For example, consider the case of pulsing subfaults: in this case the corner frequencies for each subfault will be lower than for the static case. But the original EXSIM assumes that the subfault source duration is given by equation (7); this duration is shorter than given by equa-

tion (8), resulting in the different durations seen in the first and third rows of the figure. Because the FAS are very similar, the PSV shown in Figure 8 using the shorter original duration is higher than when the duration is assumed to be the inverse of the corner frequency.

The durations for the 100 hypocenters are shown in Figure 10 for the three subfault-duration, corner-frequency combinations used in Figures 8 and 9. The durations are relatively independent of the hypocenter locations; therefore, the time series shown in Figure 9 are fairly representative of the relative durations.

The SMSIM results have also been included in Figures 8, 9, and 10. From those figures it is clear that the SMSIM results are closest to those for EXSIM when a 50% pulsing area and a duration given by equation (8) are used. (I have not experimented extensively with other pulsing-area percentages, but limited experience with EXSIM suggests that the

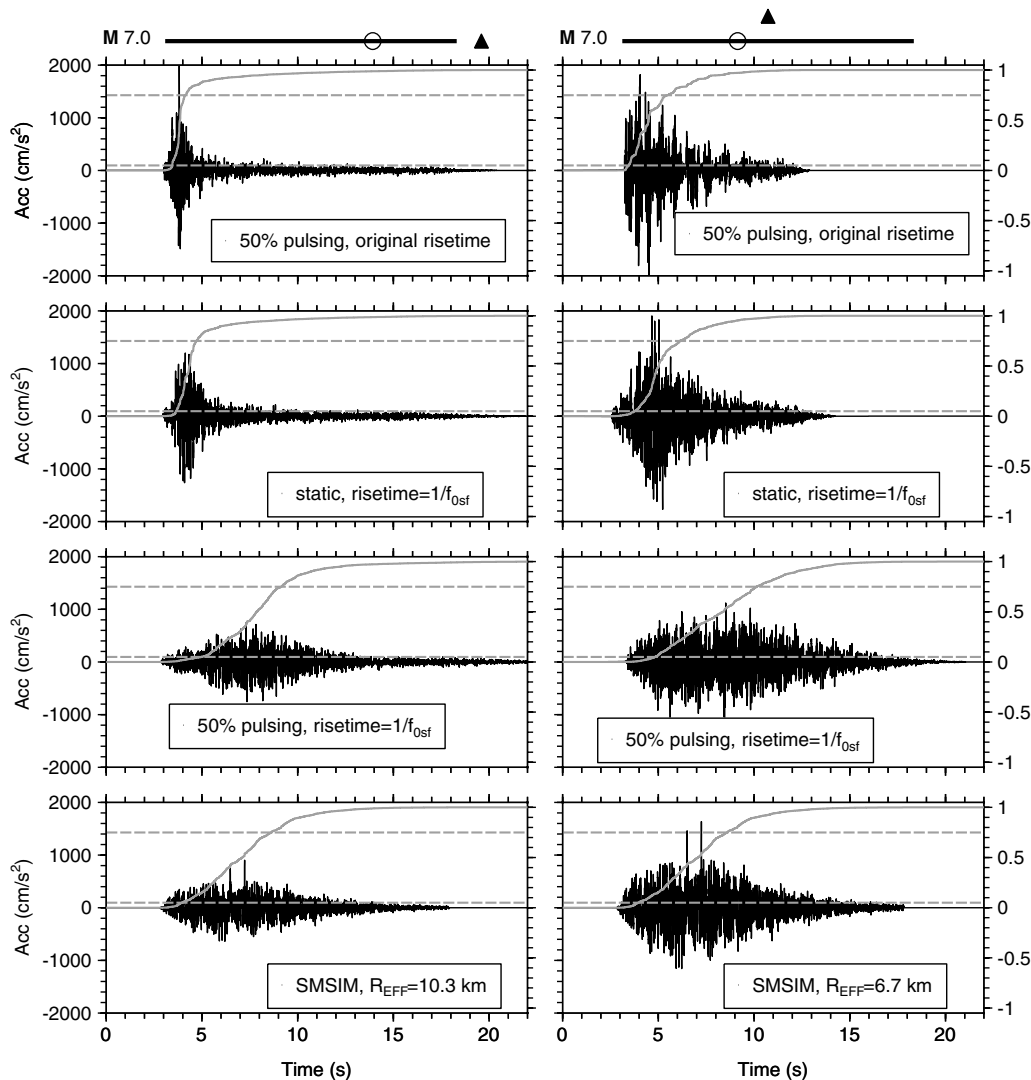


**Figure 9.** Sample acceleration time series for sites close to an  $M 7$  earthquake. The first three graphs in each column show acceleration time series computed using EXSIM with the corner frequency and rise time options as indicated; the graphs in the bottom row were computed using SMSIM with the effective distances appropriate for the site location relative to the fault. Also shown are the normalized Husid plots (cumulative squared acceleration), with horizontal lines drawn at values of 0.05 and 0.75; the durations shown in the next figure are the time interval between the 0.75 and 0.05 intersections. The relative geometries of the fault and the site are shown by the sketches at the top of the figure; the open circle is a source at the distance  $R_{\text{EFF}}$ . An exponential window was used for both the EXSIM and SMSIM calculations, with parameters  $\varepsilon = 0.2$ ,  $\eta = 0.05$ , and  $f_{\text{Tgm}} = 2.0$  (see Boore, 2003, for the meaning of these parameters).

results are not sensitive to the particular percentage used in the simulations.) It is tempting to conclude that this is the proper choice for EXSIM. But this is illogical. As in defining  $R_{\text{EFF}}$ , the proper procedure is to define an effective duration for SMSIM that mimics the effect of a finite-rupture. The problem with doing this, however, is that it is not clear what option for subfault source durations in EXSIM is most plausible physically. If I did know, then it might be possible to adjust the durations used in SMSIM to account for finite-fault size, as it is easy and quick to compute approximate envelopes for a finite fault. Although it may be serendipitous that the response spectra from SMSIM are close to the EXSIM spectra for this case, it does seem to me that the pulsing source is more physical than

the static source, and that the subfault corner frequency should be related to the inverse of the subfault duration. Based on the comparisons shown in Figures 8, 9, and 10, I suggest doing EXSIM calculations using 50% pulsing and  $1/f_{0\text{sf}}$  duration. For large distances and moderate earthquakes the choices are not important because the path component of the duration dominates the overall duration.

#### PSA from SMSIM and EXSIM Compared with Atkinson and Boore (2006)

A number of articles have been published using EXSIM to simulate motions (e.g., Motazedian and Atkinson, 2005b, c;

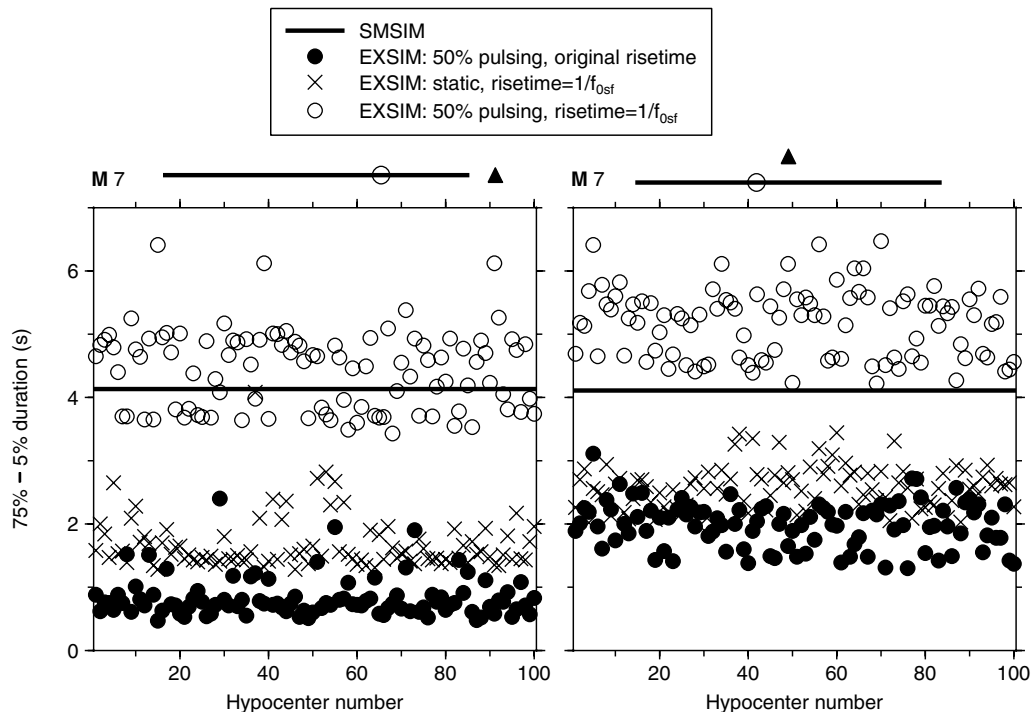


**Figure 10.** Durations between the 0.75 and 0.05 levels (Ou and Herrmann, 1990) on normalized Husid plots, for sites 2.5 km from the tip of the fault (left graph) and from the midpoint of the surface projection of the fault (right graph), for several EXSIM options for calculating subfault corner frequency and rise time. The durations are averages of 10 simulations for each of 100 hypocenters. Also shown are the averages of 300 simulations using SMSIM for the appropriate effective distance. The relative geometries of the fault and the site are shown by the sketches at the top of the figure; the open circle is a source at the distance  $R_{\text{EFF}}$ . An exponential window was used for both the EXSIM and SMSIM calculations, with parameters  $\varepsilon = 0.2$ ,  $\eta = 0.05$ , and  $f_{\text{Tgm}} = 2.0$  (see Boore, 2003, for the meaning of these parameters).

Atkinson and Boore, 2006; Motazedian, 2006; Motazedian and Moinfar, 2006). What are the implications of the revisions to EXSIM discussed in this article for those published studies? Hopefully, relatively little, if the model parameters used in those articles were calibrated against observations. Of course, I cannot repeat the analysis in the published articles, but I did compute response spectra for a relevant range of magnitudes and distances for the Atkinson and Boore (2006) model for eastern North America (this is the model used for all simulations in this article). The Atkinson and Boore (2006) motions are from equations fit to simulations for model parameters drawn randomly from statistical distributions of the parameters. As it is beyond the scope of this article to repeat that procedure, I have instead simulated motions using a fault with mean values of the parameters assumed in Atkinson and Boore (2006); the fault has a dip of  $50^\circ$ , and the motions have been simulated for many sites along lines radiating from the midpoint of the surface projection of the upper edge of the fault at azimuths ranging from  $-90^\circ$  to  $+90^\circ$ . I have compared the revised EXSIM and SMSIM simulations for these choices. Following the companion article (Atkinson *et al.*, 2009), I used a stress parameter of 250 bars; this value gives motions in rough overall agreement with the Atkinson and Boore (2006) results, but is not intended to provide an optimum fit. The median value of the stress parameter used by Atkinson

and Boore (2006) was 140 bars, based on fitting motions from eight well-recorded earthquakes in eastern North America. As shown in this article, however, two assumptions in the original version of EXSIM (the high-frequency scaling factor being based on the integral square of the Fourier velocity spectrum and the subfault duration being determined by equation 7) will lead to higher ground motions, and thus to lower inferred stress parameters, than using the revised EXSIM. The simulation results are shown in Figure 11 for azimuths of  $0^\circ$  and  $90^\circ$ ; the motions from these azimuths span those from the whole range of azimuths. It is clear that the SMSIM results are in relatively good agreement with those from the revised EXSIM with  $\Delta\sigma = 250$  bars, showing similar dependencies on the azimuth from the fault. The efficacy of using  $R_{\text{EFF}}$  rather than  $R_{\text{CD}}$  in the SMSIM simulations is also apparent from the figure.

As Atkinson *et al.* (2009) emphasize, the difference between the 140 bars used in the original version of EXSIM and the 250 bars determined here does not invalidate the Atkinson and Boore (2006) ground-motion prediction equations, as the 140 bars were determined by fitting eight well-recorded earthquakes using the original version of EXSIM. In other words, the predicted ground motions and the stress parameter used for those predictions in Atkinson and Boore (2006) are internally consistent.

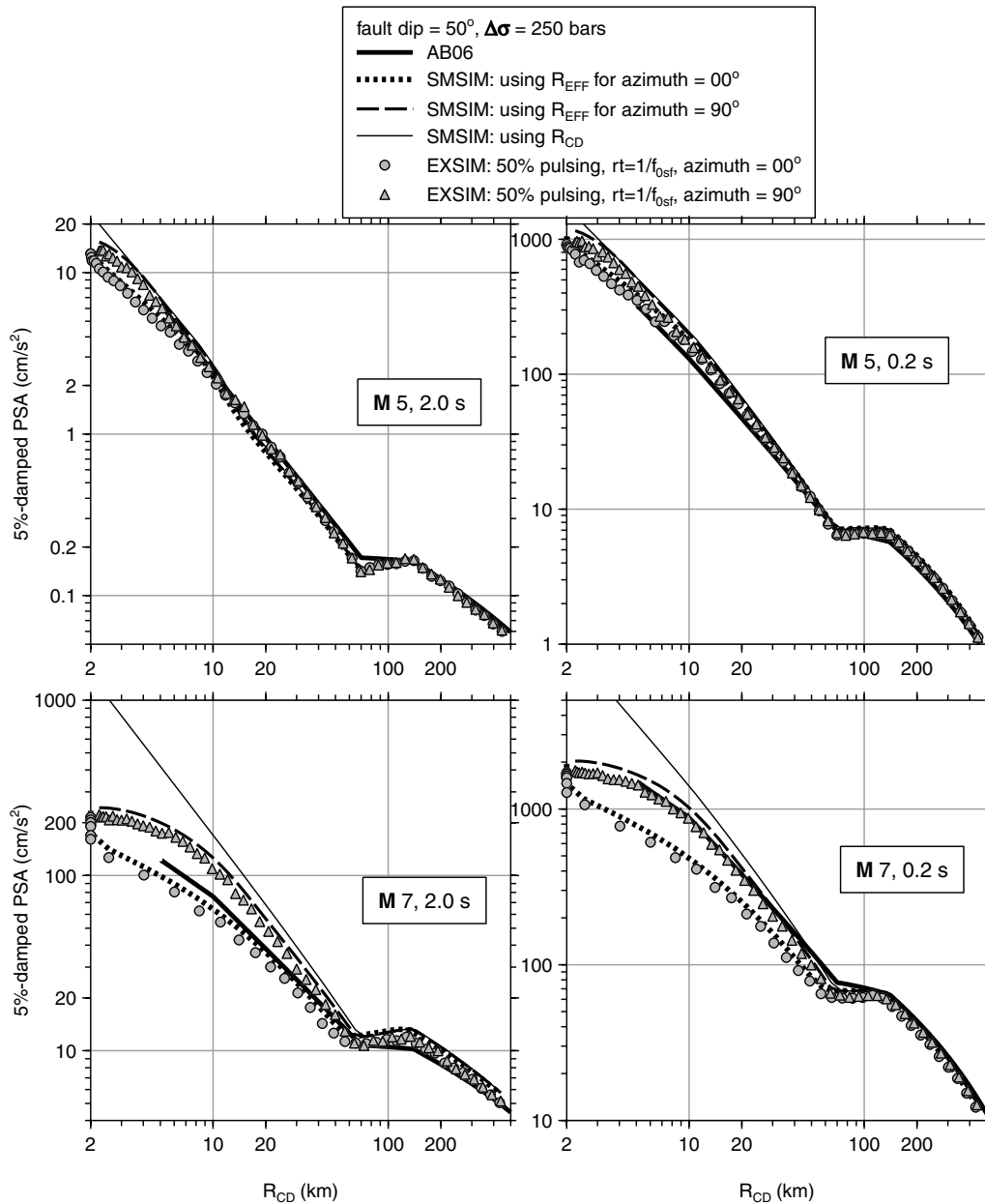


**Figure 11.** Pseudoabsolute acceleration response spectra for periods of 2.0 sec and 0.2 sec as a function of closest distance to faults dipping at  $50^\circ$ , with a depth of 2 km to the upper edge for **M 5** (top row) and **M 7** (bottom row). The sites were located along lines radiating at azimuths of  $0^\circ$  and  $90^\circ$  from the midpoint of the surface projection of the upper edge of the fault (the motions from these azimuths bracket the motions for azimuths ranging from  $-90^\circ$  to  $+90^\circ$ ). Spectra from EXSIM and SMSIM are shown, where the SMSIM runs used the appropriate effective distance for each site. For comparison, the SMSIM motions for a point source at  $R_{CD}$  and the motions from [Atkinson and Boore \(2006\)](#) are also shown.

## Discussion and Conclusions

Simple modifications were made to the point-source simulation program SMSIM and the finite-fault simulation program EXSIM. The modification to SMSIM is to use an effective distance ( $R_{EFF}$ ) that accounts for geometrical spreading and anelastic attenuation from various parts of a finite fault. Because it assumes a random distribution of hypocenters,  $R_{EFF}$  does not attempt to account for directivity

effects. This is the reason for the larger motions shown in [Figure 8](#) for a site perpendicular to the midpoint of the fault compared to motions off the tip of the fault (which would be expected to show a stronger directivity effect than at the midfault site); more of the fault is close to the midpoint and thus  $R_{EFF}$  is smaller, leading to larger motions.

A number of modifications were made to EXSIM, the most important being to use the rms of the acceleration spectra to scale the high frequencies, not to truncate the time

series from each subfault, to base the duration of the subfault motions on the inverse of the corner frequency of each subfault, and to use a filter function to boost spectral amplitudes at frequencies near and less than the subfault corner frequencies. This latter modification is required because the spectra corresponding to the time series from each subfault in the EXSIM program add incoherently, resulting in an underestimation of motion at frequencies less than the subfault corner frequencies. This effect will probably afflict any simulation method that add subfault time series with appropriate delays to account for rupture propagation, unless the low frequencies are boosted or the phase at low frequency is constrained. I note that this will not be the case for the deterministic-stochastic method of Pacor *et al.* (2005), because they do not sum subfault motions in their simulations. It will also not affect Frankel (2009), who applies a filter function similar to that used in this article. It also may not affect the motions from other broadband simulations for which the stochastic method is used only at high frequencies.

The modifications to EXSIM removed most of the differences in Fourier spectra from simulations using pulsing and static subfaults; they also essentially eliminate the remaining dependence of the EXSIM simulations on the number of subfaults (the original version of EXSIM removed the strong dependence of motions on the subfaults that existed in FINSIM, but some dependence remained, as shown here).

With the modifications previously described, the Fourier and response spectra from SMSIM and EXSIM are similar to one another, even close to a large earthquake (M 7), particularly if EXSIM is used with subfault corner frequencies based on the pulsing model and with subfault durations given by the inverse of the corner frequencies. Using an effective duration based on simple envelopes in SMSIM might result in an even better match between SMSIM and EXSIM. One important advantage of SMSIM is the speed of the calculations. The time-domain calculations are more than a factor of 10 faster than EXSIM when enough hypocenters and simulations are used to obtain a robust estimate of the motion at each site (with the difference increasing with the size of the earthquake), and the random vibration calculations are 1,000 times faster. The increase in computational speed will allow for more flexibility in exploring the effects of input parameters on the ground motion if SMSIM is used for the simulations. On the other hand, the revised SMSIM is most properly used to compute average motions from finite faults with a random distribution of hypocenters; it is not intended for calculations of motions from specific earthquakes.

The revised EXSIM requires a higher stress parameter than used in the original EXSIM in order to produce equivalent ground motions, at least at higher frequencies. For example, the Atkinson and Boore (2006) ground-motion predictions, computed using the original EXSIM with a stress parameter of 140 bars, are consistent with those computed from the revised EXSIM with a stress parameter near 250 bars.

## Data and Resources

Finite-fault versions of the random-vibration and time-domain SMSIM programs TMRS\_RV\_DRVR and TMRS\_TD\_DRVR are available from the online software link on my web site (<https://profile.usgs.gov/professional/mypage.php?name=boore>); these programs are named TMRS\_FF\_RV\_DRVR and TMRS\_FF\_TD\_DRVR. Also available from my web site is my version of EXSIM; this program is named EXSIM\_DMB.

## Acknowledgments

The seeds for this article were planted during my preparations for a course in engineering seismology taught at the ROSE School in Pavia, Italy; I thank Michele Calvi for the opportunity to give that course. The article originally was to have been a joint effort by myself, Karen Assatourians, Gail Atkinson, Ken Campbell, and Dariush Motazedian, but the work evolved in ways none of us could foresee; the originally envisioned article has been published as a companion article to this article (Atkinson *et al.*, 2009). I thank all of these people for providing feedback on the various incarnations of this article. I thank Gabriele Ameri, Gail Atkinson, Ken Campbell, John Douglas, Art Frankel, Erol Kalkan, and Dariush Motazedian for careful reviews of this article and Jack Boatwright and Walt Silva for reminding me of the Irikura and Kamae and the Ou and Herrmann references, respectively.

## References

- Ameri, G., F. Gallovič, F. Pacor, and A. Emolo (2009). Uncertainties in strong ground-motion prediction with finite-fault synthetic seismograms: An application to the 1984 M 5.7 Gubbio, central Italy, earthquake, *Bull. Seismol. Soc. Am.* **99**, 647–663.
- Andrews, D. J. (2001). A suggestion for fitting ground-motion attenuation near an extended earthquake source, *Seism. Res. Lett.* **72**, 454–461.
- Atkinson, G. M. (2004). Empirical attenuation of ground-motion spectral amplitudes in southeastern Canada and the northeastern United States, *Bull. Seismol. Soc. Am.* **94**, 1079–1095.
- Atkinson, G. M., and D. M. Boore (2006). Earthquake ground-motion prediction equations for eastern North America, *Bull. Seismol. Soc. Am.* **96**, 2181–2205.
- Atkinson, G. M., D. M. Boore, K. Assatourians, K. W. Campbell, and D. Motazedian (2009). A guide to differences between stochastic point source and stochastic finite fault simulations, *Bull. Seismol. Soc. Am.* **99**, 3192–3201.
- Beresnev, I. A., and G. M. Atkinson (1998). FINSIM—A FORTRAN program for simulating stochastic acceleration time histories from finite faults, *Seism. Res. Lett.* **69**, 27–32.
- Boore, D. M. (1983). Stochastic simulation of high-frequency ground motions based on seismological models of the radiated spectra, *Bull. Seismol. Soc. Am.* **79**, 1865–1894.
- Boore, D. M. (2003). Prediction of ground motion using the stochastic method, *Pure and Applied Geophysics* **160**, 635–676. Available from the online publications link on <https://profile.usgs.gov/professional/mypage.php?name=boore>.
- Boore, D. M. (2005a). SMSIM—Fortran Programs for Simulating Ground Motions from Earthquakes: Version 2.3—A Revision of OFR 96-80-A, *U.S. Geol. Surv. Open-File Report 00-509*, revised 15 August 2005, 55 pp. Available from the online publications link on <https://profile.usgs.gov/professional/mypage.php?name=boore>.
- Boore, D. M. (2005b). On pads and filters: Processing strong-motion data, *Bull. Seismol. Soc. Am.* **95**, 745–750.
- Cocco, M., and J. Boatwright (1993). The envelopes of acceleration time histories, *Bull. Seismol. Soc. Am.* **83**, 1095–1114.

- Frankel, A. (1995). Simulating strong motions of large earthquakes using recordings of small earthquakes: The Loma Prieta mainshock as a test case, *Bull. Seismol. Soc. Am.* **85**, 1144–1160.
- Frankel, A. (2009). A constant stress-drop model for producing broadband synthetic seismograms: Comparison with the Next Generation Attenuation relations, *Bull. Seismol. Soc. Am.* **99**, 664–680.
- Graves, R., and A. Pitarka (2004). Broadband time history simulation using a hybrid approach, in *Proc. of 13th World Conf. on Earthquake Engineering*, Vancouver, British Columbia, 1–6 August 2004.
- Hartzell, S., S. Harmsen, A. Frankel, and S. Larsen (1999). Calculation of broadband time histories of ground motion: Comparison of methods and validation using strong-ground motion from the 1994 Northridge earthquake, *Bull. Seismol. Soc. Am.* **89**, 1484–1504.
- Hisada, Y. (2008). Broadband strong motion simulation in layered half-space using stochastic Green's function technique, *J. Seismol.* **12**, 265–279.
- Irikura, K., and K. Kamae (1994). Estimation of strong ground motion in broad-frequency band based on a seismic source scaling model and an empirical Green's function technique, *Annali di Geofisica* **37**, 1721–1743.
- Joyner, W. B., and D. M. Boore (1986). On simulating large earthquakes by Green's-function addition of smaller earthquakes, in *Earthquake Source Mechanics*, American Geophysical Union Monograph **37**, 269–274.
- Mai, P. M., P. Spudich, and J. Boatwright (2005). Hypocenter locations in finite-source rupture models, *Bull. Seismol. Soc. Am.* **95**, 965–980, doi [10.1785/0120040111](https://doi.org/10.1785/0120040111).
- Motazedian, D. (2006). Region-specific key seismic parameters for earthquakes in northern Iran, *Bull. Seismol. Soc. Am.* **96**, 1383–1395.
- Motazedian, D., and G. M. Atkinson (2005a). Stochastic finite-fault modeling based on a dynamic corner frequency, *Bull. Seismol. Soc. Am.* **95**, 995–1010.
- Motazedian, D., and G. M. Atkinson (2005b). Earthquake magnitude measurements for Puerto Rico, *Bull. Seismol. Soc. Am.* **95**, 725–730, doi [10.1785/0120040083](https://doi.org/10.1785/0120040083).
- Motazedian, D., and G. M. Atkinson (2005c). Ground-motion relations for Puerto Rico, *Special Paper 385, Geological Society of America*, 61–80.
- Motazedian, D., and A. Moinfar (2006). Hybrid stochastic finite fault modeling of 2003, *M* 6.5, Bam earthquake (Iran), *J. Seism.* **10**, 91–103.
- Ohno, S., T. Ohta, T. Ikeura, and M. Takemura (1993). Revision of attenuation formula considering the effect of fault size to evaluate strong motion spectra in near field, *Tectonophysics* **218**, 69–81.
- Ou, G.-B., and R. B. Herrmann (1990). Estimation theory for strong ground motion, *Seism. Res. Lett.* **61**, 99–107.
- Pacor, F., G. Cultrera, A. Mendez, and M. Cocco (2005). Finite fault modeling of strong ground motions using a hybrid deterministic-stochastic approach, *Bull. Seismol. Soc. Am.* **95**, 225–240.
- Scherbaum, F., F. Cotton, and H. Staedtke (2006). The estimation of minimum-misfit stochastic models from empirical ground-motion prediction equations, *Bull. Seismol. Soc. Am.* **96**, 427–445, doi [10.1785/0120050015](https://doi.org/10.1785/0120050015).
- Singh, S. K., M. Ordaz, J. G. Anderson, M. Rodriguez, R. Quaas, E. Mena, M. Ottaviani, and D. Almora (1989). Analysis of near-source strong-motion recordings along the Mexican subduction zone, *Bull. Seismol. Soc. Am.* **79**, 1697–1717.

## Appendix

### Initial Modifications to EXSIM

The program EXSIM, based on the article by [Motazedian and Atkinson \(2005a\)](#), was publically available from <http://http-server.carleton.ca/~dariush/research/research.html> for a number of years. The version I used in this article was release version 1.0, 10 October 2005. In running this program I found several things that needed modification in order to make a fair comparison with the SMSIM results. As these do not pertain to the fundamental theory contained in [Motazedian and Atkinson \(2005a\)](#), I discuss these modifications here rather than in the text. My modification of

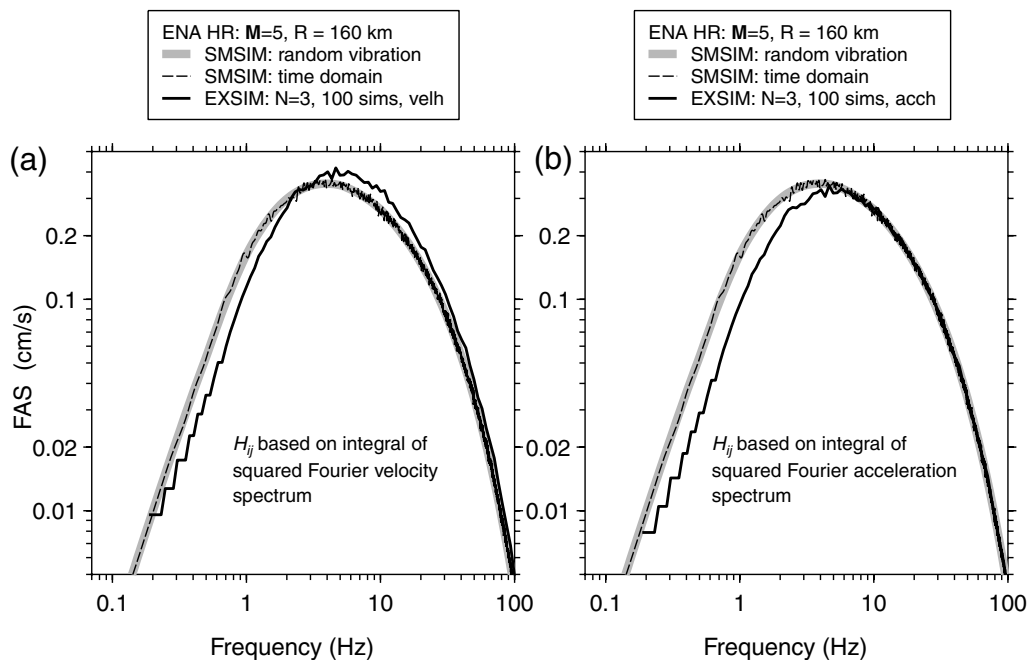


**Figure A1.** Fourier acceleration spectra, using the scaling factor  $H_{ij}$  based on (a) the integral squared velocity spectrum; and (b) the integral squared acceleration spectrum.

the program is available from the online software link on my web page: <http://quake.usgs.gov/~boore>.

### The High-Frequency Scaling Factor

In EXSIM the fault is divided into  $N$  subfaults, each with a moment equal to the moment of the event to be simulated (the target event) divided by  $N$ . The source spectrum from subfault  $ij$  is multiplied by a scale factor  $H_{ij}$ . In the distributed version of the program the scale factor is determined by requiring the integral of the squared subfault velocity spectrum to be  $1/N$  that of the integral of the squared target spectrum (treated as a point source). Figure A1a shows the comparison of the Fourier acceleration spectrum (FAS) computed from the distributed EXSIM and SMSIM, for a small earthquake ( $M$  5) at a distance much larger than the source size (160 km). In this and all other simulations in this article, the parameters are those corresponding to the eastern North American hard-rock model of Atkinson and Boore (2006). The parameters are given in Tables 1 and 2. There is clearly a mismatch in the two FAS, although for this magnitude and distance I would expect much closer agreement. Such agreement at high frequencies can be obtained if the scaling factor is based on the integral of the square of the acceleration, as shown in Figure A1b (in the main body of the article I discuss a modification that results in agreement at lower frequencies). It is my opinion that the proper scaling factor to use in EXSIM should be computed from the integral of the squared acceleration, as this gives agreement at high frequencies with the SMSIM results, and it is at high frequencies that I expect the stochastic method that is the basis of both SMSIM and EXSIM to be most applicable. I use the acceleration-based scaling factor for the rest of the simulations shown in this article. The mismatch at intermediate to low frequencies shown in both Figures A1a and A1b is discussed in the main body of the article.

A good approximation to the scaling factor based on the squared acceleration spectrum is given by the simple equation

$$H = \sqrt{N}(f_0/f_{0sf})^2, \quad (A1)$$

where  $f_0$  and  $f_{0sf}$  are the corner frequencies of the target event and the subfault, respectively (note that  $f_{0sf}$  and thus  $H$  will generally differ for each subfault; I have omitted the subfault indices for clarity). This equation is based on the assumptions that the high-frequency spectral level of the simulated event is equal to the incoherent summation of the subfault motions and that this level should equal the high-frequency level of the target event. In my revision of EXSIM the integral of the squared acceleration spectrum is computed numerically, but the results are almost identical to using equation (A1).

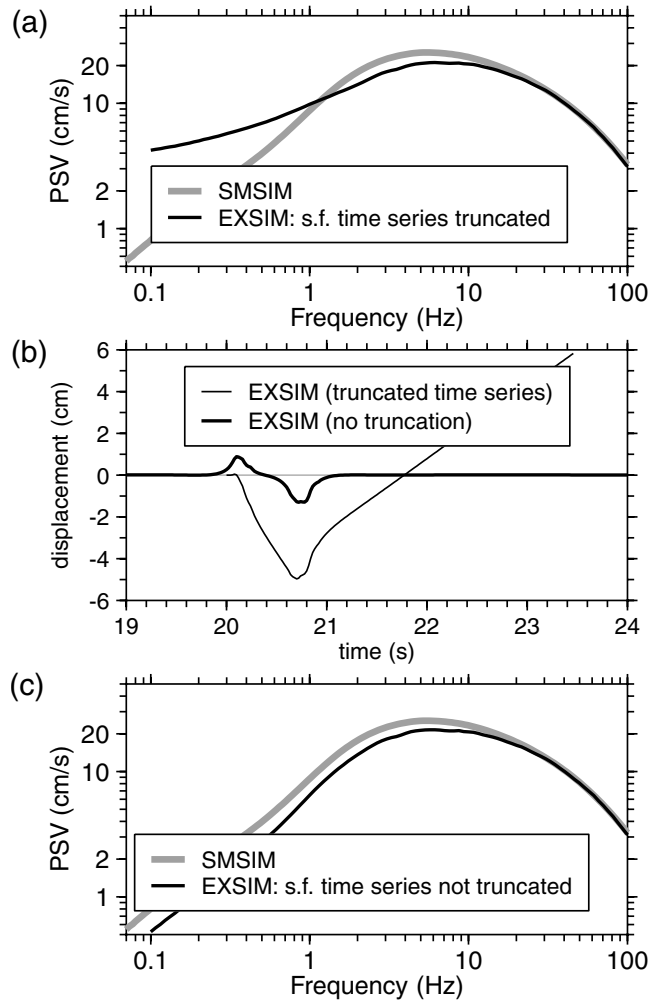


**Figure A2.** (a) Fourier acceleration and response spectrum from the distributed version of EXSIM (but using a scale factor based on the integral acceleration spectra), with SMSIM results for comparison, for  $M$  5 at 2.5 km along the perpendicular bisector of the fault. The SMSIM calculations were for an effective distance of 2.7 km, calculated using the algorithm discussed in the main body of this article (s.f.: subfault). (b) Displacements obtained from double integration of one realization of the EXSIM simulated acceleration for  $M$  5 at 2.5 km, from the distributed version of the program and my modification (in which the subfault time series is not truncated). (c) As in (a), but using my modification of the distributed version of EXSIM with no truncation of the subfault time series.

### Truncation of Subfault Time Series

Response spectra from EXSIM for small magnitudes and close distances have the wrong low-frequency slope, as shown in Figure A2a. Because the low-frequency behavior of a pseudovelocity response spectrum (defined as  $\omega SD$ , where  $SD$  is the displacement response spectrum) is controlled by the peak displacement, the most likely explanation for the decreasing slope in the PSV at low frequencies is a peak displacement that is larger than expected. Figure A2b

shows that the displacement time series from the original version of EXSIM has a strong drift that results in very large peak displacements, thus leading to the erroneous trends in PSV at low frequencies. The drift can be removed by post-processing of the time series, but a cleaner solution is based on understanding the source of the drift. I speculated that this drift is caused by the truncation of the time series from each subfault time series in the distributed version of EXSIM (i.e., there are no zero pads to accommodate the filter transients implicit in the time-domain stochastic-method process, resulting in the same type of long-period errors that can be introduced in processing accelerogram data if pads are not included (Boore, 2005b)). I modified EXSIM so that the subfault time series are not truncated; the displacement time series no longer have the long-period trends (Figure A2b), and the low-frequency PSV is well behaved (Figure A2c).

### Miscellaneous

I made several other modifications to EXSIM. Two of these modifications involve the calculation of the subfault

corner frequency and rise time; these are discussed in the main text. Another modification is a choice in the type of averages used for FAS and response spectra; as this modification did not result in important differences in the simulated motions, results using the various choices are not illustrated here. The modifications to EXSIM also apply to FINSIM, as much of the EXSIM code was based on the FINSIM code (D. Motazedian, written commun., 2009). More details regarding the changes that I made to the program are included in the comments section of the source code.

U.S. Geological Survey  
MS 977 345 Middlefield Road  
Menlo Park, California 94025  
boore@usgs.gov

Manuscript received 25 February 2009